Terrestrial gamma ray flashes with energies up to 100 MeV produced by nonequilibrium acceleration of electrons in lightning

Sebastien Celestin,[1] Wei Xu,[1] and V. P. Pasko[1]

Received 16 January 2012; revised 6 March 2012; accepted 27 March 2012; published 16 May 2012.

[1] Using Monte Carlo models simulating energetic electrons in inhomogeneous electric field and the transport of energetic photons in the Earth's atmosphere, we show that the spectrum of bremsstrahlung photons generated by nonequilibrium energetic electrons produced during stepping of lightning leaders can deviate from the typical spectrum of relativistic runaway electron avalanches (RREA) developing in weak homogeneous electric fields. This deviation is especially pronounced in the high-energy tail of the electron energy distribution for lightning leaders possessing high voltages (several hundreds of megavolts) and extremely high fields around their tips. The photon spectrum obtained accurately reproduces the recently discovered high-energy tail (up to 100 MeV) of terrestrial gamma-ray flashes (TGFs). This analysis provides the first direct evidence that TGFs are produced by lightning and not over large distances in weak thunderstorm electric fields.

Citation: Celestin, S., W. Xu, and V. P. Pasko (2012), Terrestrial gamma ray flashes with energies up to 100 MeV produced by nonequilibrium acceleration of electrons in lightning, *J. Geophys. Res.*, *117*, A05315, doi:10.1029/2012JA017535.

1. Introduction

[2] Terrestrial gamma-ray flashes (TGFs) are bursts of high-energy photons originating from the Earth's atmosphere in association with thunderstorm activity. TGFs were serendipitously discovered by BATSE detector aboard the Compton Gamma-Ray Observatory originally launched to perform observations of celestial gamma-ray sources [*Fishman et al.*, 1994]. These events have also been detected by the Reuven Ramaty High Energy Solar Spectroscopic Imager (RHESSI) satellite [*Smith et al.*, 2005], the Astrorivelatore Gamma a Immagini Leggero (AGILE) satellite [*Marisaldi et al.*, 2010], and the Fermi Gamma-ray Space Telescope [*Briggs et al.*, 2010]. Measurements have correlated TGFs with initial development stages of normal polarity intracloud lightning that transports negative charges upward (+IC) [*Stanley et al.*, 2006; *Shao et al.*, 2010; *Lu et al.*, 2010, 2011]. *Connaughton et al.* [2010] and *Cummer et al.* [2011] have shown a close association between TGFs detected by the Fermi-GBM and fast lightning processes within several tens of microseconds. Moreover, *Tavani et al.* [2011] have recently reported that the high-energy part (>30 MeV) of the TGF spectrum, measured by the AGILE mission for the first time, significantly deviated from spectra corresponding to well-established model of relativistic runaway electron avalanches (RREAs), which so far provided a very good agreement with observations at lower energies [*Dwyer and Smith*, 2005]. Additionally, *Tavani et al.* [2011] discovered photons in the high-energy tail of terrestrial gamma-ray flashes with energies up to 100 MeV (see Figure 1b).

[3] In addition to space-based measurements, X-ray and gamma-ray bursts have also been observed recently during natural and rocket-triggered lightning discharges [e.g., *Moore et al.*, 2001; *Dwyer et al.*, 2003, 2004, 2005; *Smith et al.*, 2011]. The observed X-ray and gamma-ray bursts have been linked to the production of high-energy electrons, so-called runaway electrons, in the Earth's atmosphere [*Fishman et al.*, 1994]. Runaway electrons are electrons with high energy and therefore low probability of collision with gas molecules, propagating in an applied electric field so that the energy they acquire from the field is higher than the energy losses due to collisions. These electrons are therefore capable of efficiently gaining energy from an electric field in air. One can distinguish between thermal runaway processes, for which a very high electric field E exceeds the friction force at low-energy ($\sim$100 eV) and brings electrons to regimes where they continuously accelerate ($E > E_c \simeq 240$ kV/cm in air at ground pressure), and relativistic runaway processes [*Gurevich et al.*, 1992] for which initial high-energy electrons are already present (e.g., cosmic ray secondary electrons) and can initiate relativistic runaway electron avalanches (RREAs) in electric fields higher than $E_t \simeq 2.8$ kV/cm in air at ground pressure [*Dwyer*, 2008].

[4] X-ray bursts from lightning discharges have been clearly identified to stem from the production of thermal runaway electrons [*Dwyer*, 2004] and TGFs have been suggested to be related to thermal runaway processes in lightning leader tips [*Moss et al.*, 2006]. However, until recently, TGF

[1]Communications and Space Sciences Laboratory, Department of Electrical Engineering, Pennsylvania State University, University Park, Pennsylvania, USA.

Corresponding author: S. Celestin, Communications and Space Sciences Laboratory, Department of Electrical Engineering, Pennsylvania State University, 227 Electrical Engineering East, University Park, PA 16802-2706, USA. (sebastien.celestin@psu.edu)

0148-0227/12/2012JA017535

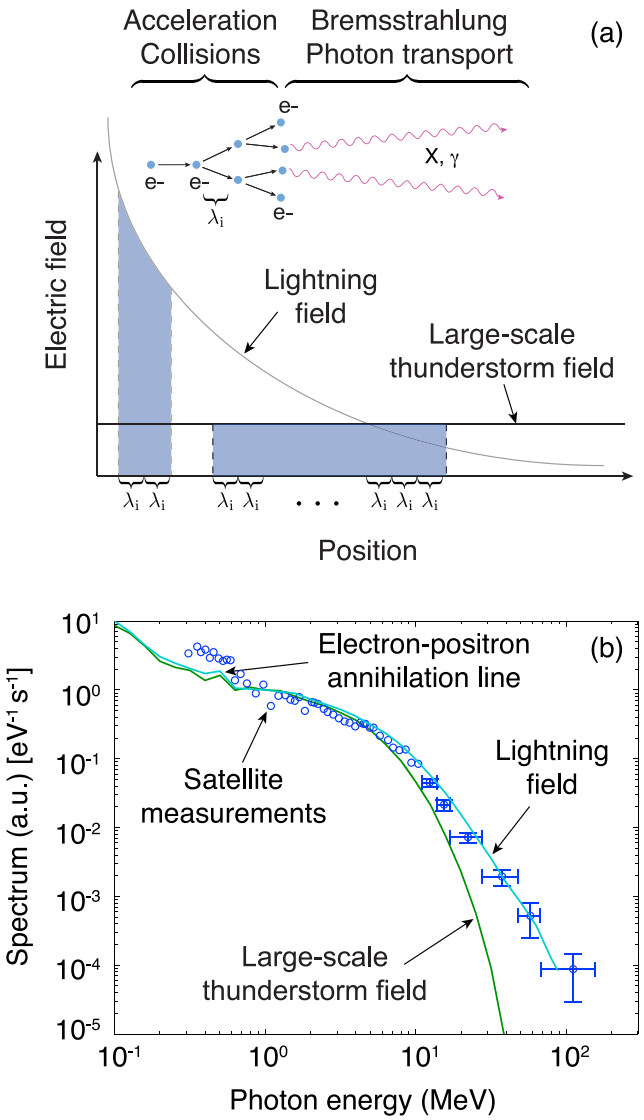

Figure 1. Acceleration and multiplication of electrons, and photon spectra. (a) Illustration of acceleration and multiplication of electrons in homogeneous and inhomogeneous fields. The electron-impact ionization process is represented with a characteristic length λ_i. For a given electron maximum energy (shaded areas), different energy distributions are expected between the homogeneous and inhomogeneous field cases because the corresponding distances of acceleration are associated with a different number of ionization lengths. (b) Spectrum at satellite altitude. Circles with error bars are reproduced from [*Tavani et al.*, 2011]. The spectrum produced in association with classical RREA process in weak thunderstorm fields (Figure 2a) is represented in green, and the spectrum obtained from the mechanism of direct acceleration in inhomogeneous lightning field (Figure 2b) is shown in blue.

spectra were very well reproduced by RREA models involving acceleration of runaway electrons in large-scale (hundreds of meters) weak electric fields in thunderstorms [*Dwyer and Smith*, 2005]. Since the number of energetic seed electrons involved in TGF production was shown to be too high to be initiated by natural background radiation or extensive cosmic-ray air showers alone, relativistic feedback mechanisms and energetic electrons seeding by lightning discharges were invoked [*Dwyer*, 2008]. The RREA processes have then been understood to provide an amplification factor of $\sim 10^5$ in the number of energetic electrons to reach a total number of $\sim 10^{17}$ energetic electrons (calculated at ~15 km altitude) believed to produce TGFs through the bremsstrahlung process [*Dwyer and Smith*, 2005; *Carlson et al.*, 2009]. The great majority of secondary electrons produced by electron-impact ionization are low energy electrons, therefore, such an amplification in the total number of energetic electrons ($\sim 10^5$) is necessarily accompanied by a marginalization of the most energetic electrons, which drive the relativistic avalanche (see section 4.1.1). This produces a characteristic high-energy ($\gtrsim$10 MeV) cutoff on the electron energy distribution function that creates a clear signature on the photon spectrum associated with the RREA process, which is weakly influenced by ambient conditions such as electric field or gas density [e.g., *Babich et al.*, 2004; *Dwyer and Smith*, 2005]. The lower energy part of the photon spectrum (<10 MeV) mostly depends on the air density (altitude) at the electron source location [*Dwyer and Smith*, 2005].

[5] In the present paper, we demonstrate that strong acceleration of a large number of thermal runaway electrons [*Celestin and Pasko*, 2011] in very strong and highly inhomogeneous electric fields of lightning discharge naturally explains the significant deviation from the RREA equilibrium at energies >30 MeV recently reported by *Tavani et al.* [2011]. We show that the spectrum of bremsstrahlung photons propagated in the atmosphere up to satellite altitude can reproduce the recent observations in the high-energy range. This analysis provides the first direct evidence that TGFs are produced by lightning and not over large distances in weak thunderstorm electric fields.

2. Model Formulation

2.1. Method of Moments

[6] We use the method of moments [*Balanis*, 1989, p. 670] in order to calculate the electric field in the vicinity of a +IC lightning negative leader tip at the very beginning of the so-called corona flash. The negative corona flash corresponds to the production of a powerful streamer corona right after the completion of a new leader step [*Bazelyan and Raizer*, 2000, p. 199] and the extreme electric fields produced in the streamer heads during the corona flash are responsible for the production of thermal runaway electrons [*Moss et al.*, 2006; *Celestin and Pasko*, 2011]. The method of moments allows for computing the electric field produced by an equipotential perfectly conducting leader channel of length l immersed in an ambient thundercloud electric field E_0. The method of moments is a quasi-static approximation, which is valid only if the electric potential in the new leader step rises fast enough so that the electric field is not shielded. In *Carlson et al.* [2010], an attempt has been made to describe a similar system using time domain simulations.

[7] Specifically, the method of moments is used to invert the integral equation of the electric potential in order to solve for the charge distribution along the leader channel. The

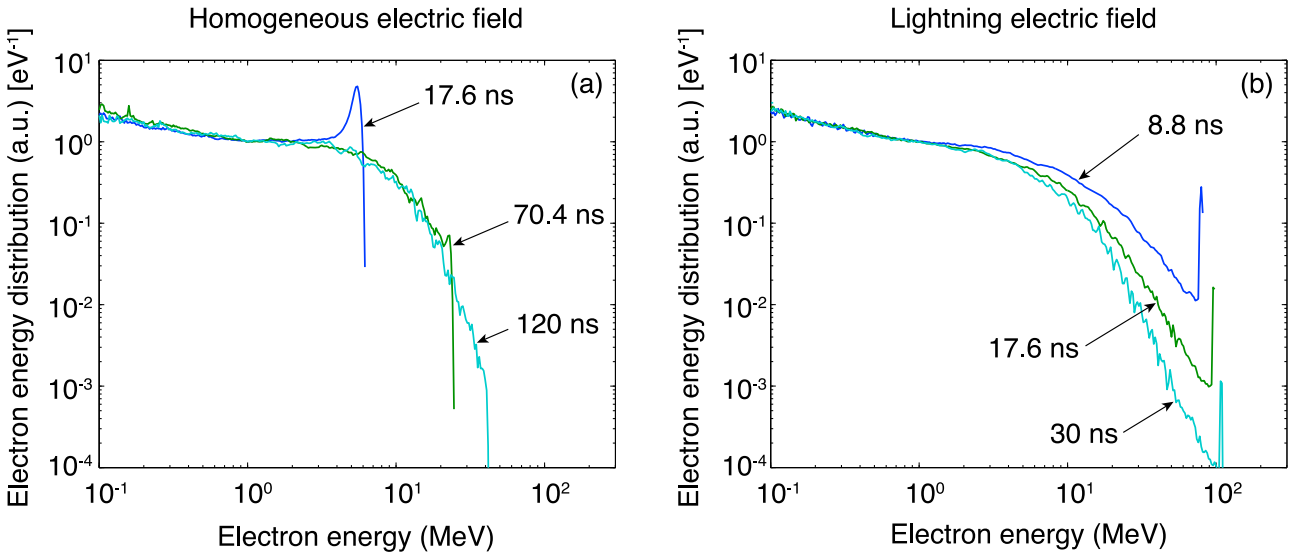

Figure 2. Electron energy distributions. (a) Electron energy distributions obtained for 3 different times in the case of propagation in a homogeneous electric field of magnitude 12.5 kV/cm. The progression of the energy distribution dynamically follows the classical steady state RREA distribution, which weakly depends on the magnitude of the external electric field. (b) Electron energy distributions obtained for 3 different times in the case of propagation in a strongly inhomogeneous electric field produced in the vicinity of a lightning leader tip. The lightning length is taken as $l = 3.5$ km and the ambient large-scale thunderstorm electric field has a magnitude $E_0 = 2 \times 10^5$ V/m. The results have been obtained in air at ground level atmospheric density. The dynamics of the electron energy distribution in this case is very transient. Differences between electron distributions shown in Figures 2a and 2b are associated with the deviation from the RREA spectrum observed by the AGILE satellite [*Tavani et al.*, 2011] and represented in Figure 1b.

charge is distributed so that the electric potential in the leader compensates the ambient potential variation due to E_0, preserving equipotentiality of the leader channel. Once the charge density is obtained, the electric field produced by the leader channel can be easily calculated. The electric potential of one lightning leader tip with respect to the ambient potential is approximately $U_1 = E_0 l/2$ [*Bazelyan and Raizer*, 2000, p. 54]. The ambient large-scale thunderstorm electric field is taken as $E_0 = 2 \times 10^5$ V/m [e.g., *Marshall et al.*, 1995]. The radius of the leader channel is chosen as 10 cm [e.g., *Rakov and Uman*, 2003, section 4.4.6, p. 134], and the IC lightning length is $l = 3.5$ km. Beyond the initial location of electrons in our code ($r \geq 0.15$ m, where r is the distance from the leader tip) the electric field can be approximated by a A/r function. For the set of parameters chosen in this study, $A \simeq 27.5$ MV represents correctly the electric field within 20% and is especially accurate in the highly inhomogeneous region close to the lightning leader tip. More generally, we find that $A(U_l) = 0.04 E_0 l = 0.04 \times 2U_l$ offers a good representation (within 20%) of the electric field in the lightning leader tip region for a wide range of voltages (or correspondingly product of ambient electric field and lightning length) from $U_1 \simeq 50$ MV to ~500 MV, with E_0 varying from 0.5 kV/cm to 3 kV/cm, with a better agreement as l increases from 2 km to 3 km.

[8] It is important to note that cloud-to-ground lightning discharges usually exhibit extensive branching that leads to a significant reduction of the lightning electric potential [*Bazelyan and Raizer*, 2000, p. 166], preventing these discharges from producing the extremely energetic radiation studied in the present article [*Celestin and Pasko*, 2011].

2.2. Monte Carlo Model for Electrons

[9] The Monte Carlo model we have developed simulates the propagation and collisions of electrons in air (80% N_2 and 20% O_2) under an applied electric field [*Celestin and Pasko*, 2011]. This model is three-dimensional (3-D) in the velocity space, 3-D in the configuration space, relativistic, and simulates electrons from sub-eV to GeV. For the energy range considered in this work (10^4 to 2×10^8 eV) only ionization and elastic scattering are significant. The singly differential cross sections of ionization of N_2 and O_2 are calculated over the full range of energy through the relativistic binary-encounter-Bethe model [*Kim et al.*, 2000; *Celestin and Pasko*, 2010]. The knowledge of this differential cross section allows for obtaining the energy of the secondary electrons [*Moss et al.*, 2006] after ionizing collisions. The scattering angles of primary and secondary electrons are then obtained from the relativistic equations of conservation of momentum and energy considering that the newly formed ion is static. Since electrons with very high energy (~100 MeV) are involved in our calculations, we introduce a continuous radiative friction of electrons due to bremsstrahlung [*Berger et al.*, 2005].

2.3. Monte Carlo Model for Photons

[10] From the knowledge of the time evolution of the electron energy distribution function (see further discussion of Figures 2a and 2b) and the bremsstrahlung differential cross section [*Lehtinen*, 2000, chapter 3.2], one can calculate the photon spectrum produced by the electrons. The source is chosen with a broad beam geometry (isotropic within a 45° angle) at 15 km altitude, that is believed to be typical of TGFs

[*Dwyer and Smith*, 2005; *Carlson et al.*, 2007; *Østgaard et al.*, 2008]. Note that *Gjesteland et al.* [2011] have recently found beaming angles within 30°–40° to be likely. We model the photon transport in the atmosphere up to 500 km, that is the typical altitude of low-orbit satellites detecting TGFs [*Fishman et al.*, 1994; *Smith et al.*, 2005; *Marisaldi et al.*, 2010; *Briggs et al.*, 2010], using a dedicated Monte Carlo code. We note that in the present work the satellite altitude is not critical since we do not perform a spatial parametric study of TGF source location with respect to the satellite location, and one can safely consider that no collisions between photons and air molecules occur above ∼100 km altitude. The differences between simulation results and measurements in the lower energy part of the photon spectrum (see further discussion of Figure 1b) are mainly due to the response of the detector, and the altitude and geometry of the source [e.g., *Dwyer and Smith* 2005]. Since the AGILE's detector response matrix is not publicly available, in the present work, we do not perform a direct model/measurement comparison of the lower energy part of the spectrum (≤5 MeV). The Monte Carlo model for photons takes into account the relevant collisions between photons and air molecules for the energy range considered, similarly to works widely described in the literature [*Østgaard et al.*, 2008]. Three different collision types are taken into account: Photoelectric absorption (main process for energies up to ∼30 keV), Compton scattering (main process from ∼30 keV up to ∼30 MeV) and electron-positron pair production (main process >30 MeV). As for the dynamics of photons, photoelectric absorption creates a low energy cutoff on the spectrum below ∼50 keV [*Dwyer and Smith*, 2005; *Østgaard et al.*, 2008], Compton scattering dynamically decreases the energy of photons, and pair production process produces positrons that eventually annihilate with ambient electrons producing the 511 keV annihilation line (Figure 1b). Important secondary effects (i.e., energetic electrons and positrons launched to the magnetosphere) are now recognized to be produced by Compton scattering and pair production of TGFs [*Dwyer et al.*, 2008; *Briggs et al.*, 2011]. However, since we focus primarily on the dynamics of photons in this study, positrons are considered to annihilate locally where pair production has occurred, and secondary Compton-produced electron bremsstrahlung is not taken into account [e.g., see *Østgaard et al.*, 2008]. The very good agreement obtained with previous studies [e.g., *Dwyer and Smith*, 2005; *Østgaard et al.*, 2008] justifies these simplifications.

3. Results

[11] The unexpected strong deviation from the RREA spectral signature in the high-energy part of the spectrum (>30 MeV) observed by AGILE satellite [*Tavani et al.*, 2011], as illustrated in Figure 1b, is challenging RREA-based theories of TGF production, since the TGF spectrum was precisely the main evidence of the RREA mechanism. In the following, we show that the dynamics of electrons accelerated in the vicinity of lightning leader tips can reproduce the high-energy spectrum recently uncovered [*Tavani et al.*, 2011], while acceleration of electrons in homogeneous large-scale weak electric fields (RREA process) is only able to fit the spectrum for photons with energies lower than ∼30 MeV [e.g., *Dwyer and Smith*, 2005].

[12] Figure 1a illustrates the fundamental reason behind this effect. The acceleration of electrons up to energies on the order of hundreds of MeV in large-scale weak electric fields present in thunderstorm is theoretically possible, however, as energetic electrons accelerate, they produce a large number of lower energy secondary electrons by impact ionization. In Figure 1a, this mechanism is represented with a characteristic length λ_i. Thus, a relationship exists between the total distance of acceleration undergone by the electrons and the quantity of the secondary electrons produced. In a weak electric field, the population of energetic electrons is promptly overcome by lower energy electrons that create a fast drop, or energy cutoff, in the electron energy distribution (see Figure 2a and section 4.1.1). Therefore, in the case of large-scale weak electric fields present in thunderstorms, the RREA mechanism cannot deviate from this particular energy distribution [*Babich et al.*, 2004; *Dwyer and Smith*, 2005; *Dwyer and Babich*, 2011]. Contrary to the large-scale weak electric field scenario, the inhomogeneous high electric fields naturally present in compact regions around negative lightning leader tips during stepping processes can accelerate thermal runaway electrons to high energy over a short distance, corresponding to a much lower number of impact ionization lengths (see Figure 1a) and much lower corresponding number of low-energy secondary electrons. Due to the rapid change of the electric field seen by the electrons as they are progressing in the inhomogeneous field, the equilibrium is not reached and the ensemble of electrons is intrinsically in nonequilibrium.The characteristics of electron energy distribution during transient acceleration stage near leader tips should therefore be significantly different from the RREA distribution and these characteristics are examined in the analysis that follows.

[13] Figure 2a presents the electron energy distribution of an ensemble of energetic electrons that propagate under a homogeneous electric field of magnitude 12.5 kV/cm in air at ground pressure calculated by a Monte Carlo model (see section 2.2) at different instants of time. In order to emphasize the time evolution of the energy distribution, we normalized the distributions shown in Figure 2 so that they all yield unity at 1 MeV. Therefore, electron energy distributions are represented in arbitrary units (a.u.). Thermal runaway electrons are initiated with 65 keV in the anti-parallel direction of the electric field [*Celestin and Pasko*, 2011]. Figure 2a shows the typical dynamics of electrons in the case of RREAs, and we see that the energy distribution dynamically follows the shape of the steady state distribution over time. Figure 2a also clearly shows the formation of the classical RREA energy cutoff for energies higher than ∼10 MeV. It is important to note that even for transient states of the dynamics of the electrons, in the case of reasonable magnitude of large-scale electric fields in thunderstorms ($\ll E_k \simeq$ 30 kV/cm, where E_k is the conventional breakdown threshold field defined by the equality of the ionization and dissociative attachment coefficients in air), the electron energy distribution cannot significantly depart from the RREA equilibrium. The magnitude of 12.5 kV/cm is typical of the electric field in the streamer zone of negative leaders [*Bazelyan and Raizer*, 2000, chapter 4.6]. Calculations with lower electric fields do not sensibly change this characteristic energy cutoff [*Babich et al.*, 2004; *Dwyer and Smith*, 2005; *Dwyer and Babich*, 2011]. We note that RREA electron energy

distribution presented in Figure 2a is very similar to those already published in the literature [*Babich et al.*, 2004; *Celestin and Pasko*, 2010; *Dwyer and Babich*, 2011].

[14] Negative part of a bidirectional lightning leader representative of a +IC lightning discharge is believed to propagate by steps [*Rakov and Uman*, 2003, chapter 9]. The electric field in the vicinity of the lightning leader tip is high only during negative corona flash processes [*Bazelyan and Raizer*, 2000, chapter 4.6], that are associated with the development of a step of the negative leader. In order to calculate the electric field in the vicinity of a +IC lightning negative leader tip at the very beginning of the corona flash, we used the method of moments [*Balanis*, 1989, p. 670] (see section 2.1). Physical parameters have been chosen to correspond to a realistic lightning discharge [*Rakov and Uman*, 2003] that would produce enough potential difference in its tip for electrons to reach ~100 MeV (see section 2.1). Electrons are launched 15 cm from the leader tip with 65 keV energy [*Celestin and Pasko*, 2011] in a region where the electric field is extremely inhomogeneous and high ($E \simeq A/r$). Given the extreme acceleration undergone by the electrons within a few nanoseconds, the exact energy of initial electrons does not influence any results of the present work. Figure 2b shows the normalized electron energy distribution of the ensemble of energetic electrons strongly accelerated in the highly inhomogeneous electric field of the lightning leader tip. The lower energy part (<10 MeV) of the electron distribution is very similar to that in the RREA case (Figure 2a). The higher energy part, however, differs significantly. Instead of a strong energy cutoff as obtained in the case of RREA (Figure 2a), the distribution takes a profile closer to a power law that gets steeper with time progression. As further discussed in section 4.3, the related photons at satellite altitudes possess spectral features in good agreement with those reported by *Tavani et al.* [2011]. Eventually, for long times, the distribution will dynamically converge to a classical RREA distribution type (i.e., dominated by secondary-electrons and exhibiting high energy cutoff).

4. Discussion

4.1. Electron Energy Distribution

4.1.1. Homogeneous Electric Field

[15] In the case of an RREA, it takes some time (or corresponding distance) for the ensemble of electrons to reach equilibrium and acquire the RREA distribution. To understand how the RREA distribution is formed, it is insightful to consider the average force applied to an electron subjected to the homogeneous electric field $\mathbf{E}_0$:

$$\frac{d\mathbf{p}}{dt} = q_e\mathbf{E}_0 - F_D\frac{\mathbf{p}}{p} \tag{1}$$

where $\mathbf{p}$ is the relativistic electron momentum, q_e is the charge of the electron, and F_D is the average friction due to collisions. Here we consider the case where $q_eE_0 - F_D > 0$, that is the runaway electron case. In general, the kinetic energy of the electron is:

$$\mathcal{E} = \sqrt{m_e^2c^4 + c^2p^2} - m_ec^2 \tag{2}$$

where m_e is the mass of the electron and c is the speed of light in vacuum. In the energy range of interest here (a few MeVs), the friction force is approximately constant $F_D \simeq q_eE_t \simeq$ 2.8 keV/cm [e.g., *Moss et al.*, 2006, Figure 2], and therefore, the right-hand side of equation (1) can be assumed to be constant. As a result, equation (1) gives approximately $p(t) = p_0 + (q_eE_0 - F_D)t$ and from equation (2) it is then possible to find the characteristic time dt during which the electron crosses the energy bin $d\mathcal{E}$:

$$\frac{dt}{d\mathcal{E}} = \frac{1}{\nu(q_eE_0 - F_D)} \tag{3}$$

where ν is the velocity of the electron and in the energy range considered here, $\nu \simeq c$. During its acceleration in the field E_0 the electron produces new runaway electrons by ionization collisions with a frequency ν_a tabulated in the literature [e.g., *Celestin and Pasko*, 2010, and references therein]. The number of runaway electrons follows:

$$\frac{dN_{run}}{dt} = \nu_aN_{run} \tag{4}$$

[16] Most of the secondary runaway electrons are produced with energies close to the runaway energy threshold. As this population of lower energy runaway electrons grows, the statistical importance of electrons with the highest energies decreases while they keep gaining more energy. The electron energy distribution function is defined as a quantity proportional to the number of electrons per energy interval $f(\mathcal{E},t) \propto \left|\frac{\partial N}{\partial \mathcal{E}}\right|$. Rigorously, $N(\mathcal{E},t)$ is a cumulative distribution function. Given the parametric variable s, we have

$$\frac{dN}{ds} = \frac{\partial N}{\partial t}\frac{dt}{ds} + \frac{\partial N}{\partial \mathcal{E}}\frac{d\mathcal{E}}{ds} \tag{5}$$

[17] Steady state is reached if $\frac{dN}{ds} = 0$ along the characteristic line $(t(s), \mathcal{E}(s))$ defined by $ds = dt$, and $\frac{d\mathcal{E}}{dt}$ follows the equation (3) derived for an electron. Remembering that the majority of new runaway electrons are produced at lower energies close to the runaway threshold, using equation (4) we can write

$$\frac{\partial N}{\partial t} \simeq \nu_aN \tag{6}$$

[18] Thus, when steady state is reached equation (5) gives

$$\nu_aN + \frac{\partial N}{\partial \mathcal{E}}\frac{d\mathcal{E}}{dt} \simeq 0 \tag{7}$$

[19] Substituting equation (3) into equation (7) leads to

$$\frac{\partial N}{\partial \mathcal{E}} \simeq -\frac{\nu_a}{c(q_eE_0 - F_D)}N \tag{8}$$

[20] Equation (8) simply expresses the marginalization of energetic electrons traveling in the energy space by the exponential increase of lower energy runaway electrons.

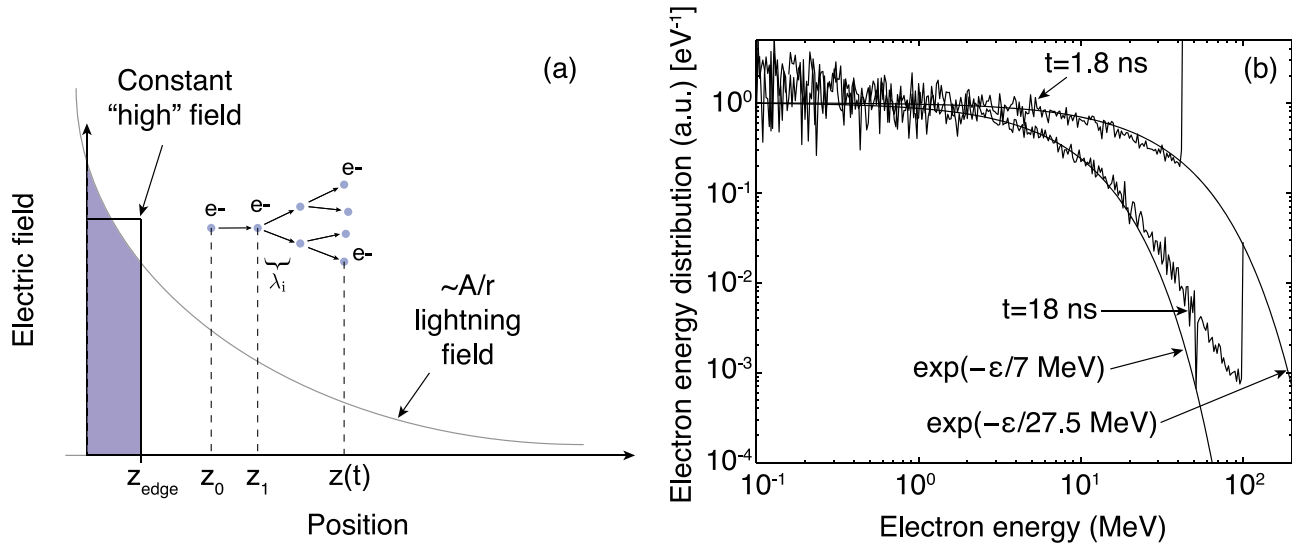

Figure 3. (a) Schematics representing the acceleration and production of electrons in electric fields. (b) Electron energy distribution functions in the inhomogeneous high electric field E = 27.5 MV/r (see section 2.1) at t = 1.8 ns and t = 18 ns. Analytical exponential functions with characteristic cutoffs 7 MeV (RREA) and 27.5 MeV (inhomogeneous field) are represented.

Indeed, during a characteristic time δt the proportion of high energy electrons drops by a factor $\nu_a \delta t$, while moving forward in the energy space by the quantity $\delta\mathcal{E} = c(q_e E_0 - F_D)\delta t$. Therefore, the exponential increase of the number of runaway electrons (equation (4)) corresponds to an exponential decrease of the electron energy distribution function in the energy space.

[21] In conclusion, the electron energy distribution in steady state can be written as

$$f(\mathcal{E}) \simeq B \exp\left(-\frac{\nu_a}{c(q_e E_0 - F_D)}\mathcal{E}\right) \tag{9}$$

where B is a normalization factor independent from $\mathcal{E}$. Note that the runaway avalanche is not going exactly at the speed of light, which introduces a small error on the order of 10% [see *Coleman and Dwyer*, 2006] in the energy cutoff $\mathcal{E}_c \simeq \frac{c(q_e E_0 - F_D)}{\nu_a}$ in equation (9). This error is negligible when describing the general shape of the energy distribution.

[22] Interestingly, the RREA rate ν_a varies almost linearly with the applied electric field E_0 and at ground air pressure can be approximated as $\nu_a \simeq 55E_0 - 3 \times 10^7$, where E_0 is in volt per meter and ν_a in s^{-1} [*Celestin and Pasko*, 2010, Figure 5, and references therein]. Therefore, the high-energy cutoff $\mathcal{E}_c$ is weakly dependent on the electric field. In the case E_0 = 12.5 kV/cm used in calculations corresponding to RREA in homogeneous fields presented in section 3, we can calculate $\mathcal{E}_c \simeq c(q_e E_0 - F_D)\nu_a^{-1} \simeq 7.5$ MeV, which is close to the simulated spectrum. For relatively high fields $q_e E_0 \gg F_D \simeq q_e E_t \simeq 2.8$ keV/cm, the high-energy cutoff can be approximated as $\mathcal{E}_c \simeq \frac{cq_e E_0}{\nu_a} \simeq \frac{cq_e}{55} \simeq 5.45$ MeV. In the above analysis, F_D and ν_a scale like N/N_0, where N is the ambient air density and N_0 is the ground level air density. Therefore, the high-energy cutoff in the steady state RREA distribution function does not depend on the density for a given reduced field E/N.

[23] Note that an analysis leading to similar results can be carried out from the Boltzmann equation [*Dwyer and Babich*, 2011, section 6].

4.1.2. Inhomogeneous Electric Field Produced by a Lightning Leader

[24] For the sake of discussion, let us assume a homogeneous electric field over a region of space between zero and z_{edge}, that falls down to zero for $z > z_{edge}$ (see Figure 3a). One can clearly see that z_{edge} can be small enough so that the RREA equilibrium is not reached by the time electrons are exiting the high-field region. The extreme limiting case, for example, is a vacuum (or sufficiently low gas density gap) that all electrons traverse and gain the maximum possible energy corresponding to the applied voltage difference. An inhomogeneous field can be approximated by a sequence of small steps, each with width z_{edge}, and therefore, in the case of a field sufficiently inhomogeneous, one can consider that the ensemble of electrons is in nonequilibrium at all time. Therefore, the distribution function would depend on the shape of the electric field (such as characteristic gradients of the electric field) as well as the effect described in the previous section.

[25] In order to draw a more quantitative picture within the context of lightning discharges and TGFs, let us consider a one-dimensional case of an electric field E produced in the vicinity of a lightning leader tip varying as A/r (see section 2.1). If the electric force is high compared with the friction force, the kinetic energy $\mathcal{E}(t)$ gained by a relativistic electron starting from $z = z_0$ can be written as

$$\mathcal{E}(z_0, t) = q_e \int_{z_0}^{z(t)} E dz = q_e A \ln(z(t)/z_0) \tag{10}$$

where q_e is the charge of the electron, t is the time, and $z(t) \simeq z_0 + ct$, where c is the speed of light in vacuum. If one assumes that the energy gained from the electric field is

much greater than the electrons original energy, equation (10) also represents the total kinetic energy of the electron. Let us assume that this electron produces a secondary energetic electron at $t = t_1$ corresponding to the position $z = z_1 = z_0 + ct_1$ (see Figure 3). For the sake of simplicity, we will assume that the electric field is high enough so that the energy gained from the field quickly overcomes the original energy of the electron. We will also consider that this secondary electron is directly produced in the relativistic regime, where its velocity is close to the speed of light (that is all the electrons considered are going at the same speed c and therefore are at the same location $z(t)$ at a given time t). This assumption along with the high-field assumption allows to get a one-to-one relationship between z_1 and $\mathcal{E}(z_1, t)$ that simplifies calculations (see equation (12) below). We can write the energy of this secondary electron with respect to time:

$$\mathcal{E}(z_1, t) = q_e A \ln((z_1 + c(t - t_1))/z_1) = q_e A \ln((z_0 + ct)/z_1) \tag{11}$$

[26] From this equation, one can calculate the energy $\mathcal{E}(z_1, t)$ of an electron knocked off at z_1 after a time t. Reciprocally, an electron with energy $\mathcal{E}(z_1, t)$ has been produced at the location:

$$z_1 = \frac{z_0 + ct}{\exp\left(\frac{\mathcal{E}(z_1,t)}{q_e A}\right)} \tag{12}$$

[27] The electron energy distribution can be written and developed as

$$f(\mathcal{E}, t) = \left|\frac{\partial N}{\partial \mathcal{E}}\right| = \left|\frac{\partial N}{\partial z} \cdot \frac{dz}{d\mathcal{E}}\right| \tag{13}$$

In this expression we can use $\frac{\partial N}{\partial z} = \alpha N = N/\lambda_i = N N_0 \sigma_i(\mathcal{E}_s > \mathcal{E}_m)$, where λ_i is a characteristic ionization length depending on the ionization cross section and the chosen threshold energy $\mathcal{E}_m$, which is in principle different from the runaway energy threshold. In this example, we chose $\mathcal{E}_m$ implicitly by assuming all electrons relativistic ($\mathcal{E}_m > 511$ keV). In reality, $\mathcal{E}_m$ is defined by the relaxation time of the electric field, since low energy electrons produced might not have time to accelerate before the collapse of the electric field. In this example, assuming all electrons with energies higher than 1 MeV also makes the cross section (or λ_i) almost independent of the energy of the primary electrons because of the relativistic plateau in this energy range. Finally, we can write the electron energy distribution function as:

$$f(\mathcal{E}, t) = \frac{z(t)\exp(z(t)/\lambda_i)}{q_e A \lambda_i} \exp\left(-\frac{\mathcal{E}}{q_e A}\right) \tag{14}$$

where the only dependance on $\mathcal{E}$ is defined by the geometrical shape of the electric field ($q_e A$). Owing to the assumptions made above, the pre-exponential factor is a simple normalization factor that does not depend on the energy. Although the present approach is too simple to reproduce the full system over time, it gives a fair representation of the distribution function for times short enough so that the variation rate of the energy of the electrons changes too quickly to be balanced by the production of runaway electrons as described in section 4.1.1 (see Figure 3b). Equation (14) suggests a distribution similar to the one produced by RREA ($\propto \exp(-\mathcal{E}/7\ \text{MeV})$) but with an energy cutoff $q_e A$ = 27.5 MeV (see Figure 3b), providing a useful analytical interpretation of exact distributions shown in Figure 2b. In particular, the transient distributions shown in Figure 2b lie between these two limiting analytical distributions.

4.2. Relaxation of the Electric Field

[28] It is important to note that we do not simulate the fully self-consistent problem, where strong ionization should eventually screen out the leader tip electric field. Nevertheless, it is possible to estimate the timescale for which the electric field in the vicinity of the lightning leader tip would be influenced by the electron density produced. Indeed, this timescale is the so-called Maxwell time $\tau_M = \varepsilon_0/q_e\mu_e n_e$, where ε_0 is the vacuum permittivity, μ_e is the electron mobility, and n_e is the electron density, which can be evaluated from our simulation results. In this configuration it is conceivable that the high field is pushed forward by the discharge in a large scale ionization wave fashion. The mechanism discussed in this article, which is based on the inhomogeneity of the electric field, and the related conclusions would not significantly change in the case of a moving field, as long as the field wave velocity is negligible compared to the speed of light. Since the high energy part of the electron distribution function is in a transient state converging to the RREA equilibrium (Figure 2b), we use the satellite measurements as a way to put a bound on the characteristic time of the collapse of the electric field and the duration of the runaway electron acceleration (Figure 1b).

[29] In the lightning case simulations, electrons are initially placed 15 cm from the leader tip where the electric field calculated using the quasi-static method of moments for a very high potential lightning leader (350 MV) is on the order of 1000 kV/cm. Whether these high fields in stepping leaders are needed to support the mechanism proposed in this paper clearly requires further investigation as they would involve very short processes in the lightning leader. Initially placing electrons at larger distances from the leader tip (lower electric field) and obtaining the hardening of the spectrum described in this paper is possible, however the total available energy over 10 m (30 ns of propagation, see section 4.3) would then be limited and even higher electric potential would have to be invoked. We emphasize that the only possibility to obtain both a very hard spectrum and a high maximum energy ($\sim$100 MeV) is to assume that extreme electric fields are present.

4.3. Comparison With Satellite Measurements

[30] We have used a Monte Carlo model in order to simulate the transport of bremsstrahlung photons produced by energetic electrons from a given source altitude (chosen to be 15 km) up to a satellite altitude of 500 km (section 2.3). Figure 1b shows the TGF spectrum for photons collected over a disk of 500 km radius and associated with the electron distributions obtained in the homogeneous field RREA case (Figure 2a) and in the case of acceleration of electrons in an

inhomogeneous lightning leader field over a time of 30 ns (Figure 2b). As in Figure 2, the calculated spectra shown in Figure 1b are normalized so that they all yield unity at 1 MeV. We note that for times much greater than $t \sim 10$ ns, the electron distribution gets closer to the RREA regime while the electron density produced becomes unphysically large. The very good agreement between measurements and model shown in Figure 1b provides evidence that the TGF spectrum may be produced during a very transient stage before the lightning field gets screened out by the tremendous production of low-energy electrons. The best agreement is found at $t = 30$ ns, however a satisfying agreement is found for $t = 30 \pm 10$ ns. We note that reported satellite measurements (Figure 1b) represent averaged data, and therefore a more accurate comparison could be achieved by averaging over different realistic lightning parameters. However, we found that these dependencies are weak compared to the deviation from the RREA regime, as long as a physical electron density produced is considered. Additionally, for a wide range of lightning parameters the electric field in the vicinity of the leader tip is found to keep the same $1/r$ shape, where r is the distance from the leader tip (see section 2.1). Note that the collapse time $t = 30 \pm 10$ ns should be considered as an order of magnitude estimate. Indeed, as a reference, the simulation results on the electron distributions have been obtained at ground pressure. The air density drops by a factor of ~7 at 15 km, and the collapse time of the electric field should increase accordingly. Nevertheless, this timescale corresponds well to measurements of current pulses associated with leader steps at low altitude [e.g., *Howard et al.*, 2011, and references therein].

[31] The dispersion timescale of the photons (light curve) in our results is on the order of ~50 μs [*Celestin and Pasko*, 2012]. The timescale of TGFs as measured by AGILE [*Marisaldi et al.*, 2010; *Tavani et al.*, 2011] is on the order of 1–5 ms, although RHESSI and Fermi measurements [*Grefenstette et al.*, 2008; *Briggs et al.*, 2010] are closer to ~0.2 ms or shorter [*Fishman et al.*, 2011]. These discrepancies in measurements prevent us from carrying out detailed comparison on TGF timescales. A possible cause of the differences in timescales is associated with the differences in instrumental dead time [*Grefenstette et al.*, 2008] and in methods different authors use in order to describe the TGF durations. Moreover, although it does not explain the differences between AGILE's and RHESSI/Fermi's results, based on the mechanism we suggest, a process related to lightning propagation might explain long TGF duration. *Lu et al.* [2011] have shown that TGFs were triggered in correlation with fast-rising high current pulses "superposed on a slow pulse that reflects a process raising considerable negative charge within 2–6 ms" and *Shao et al.* [2010] suggested that some of these fast-rising pulses are probably related to the stepping of the negative lightning leader. It is therefore conceivable that one TGF event be produced by several lightning leader steps (corresponding negative corona flashes) over a total period of 2–6 ms. If so, the time resolution of satellite detectors would not always enable possible discrimination between different gamma-ray bursts. This mechanism is also supported by the fact that multiple-pulse TGFs have been recorded since their discovery [*Briggs et al.*, 2010], and *Fishman et al.* [2011] have suggested that many of TGF pulses lasting between ~200 μs and ~1 ms might be attributed to overlapping of shorter pulses. A detailed analysis of the Compton dispersion times in the case of TGFs can be found in *Celestin and Pasko* [2012].

5. Conclusions

[32] In the present study, we demonstrate that the recently observed significant deviation of the TGF spectrum from spectra associated with relativistic runaway electron avalanches in large-scale weak electric fields present in thunderstorms, for energies greater than ~30 MeV, is the first direct evidence that TGFs are actually produced by runaway electrons strongly accelerated in highly inhomogeneous fields of +IC lightning leader. The presented mechanism is strongly supported by the observations reported in *Lu et al.* [2010, 2011], which have conclusively shown that TGFs can be produced during the upward leader stage of a +IC lightning flash. The described electron acceleration is a robust process that follows from strong electric field inhomogeneity around lightning leader tips. In order to obtain a good agreement with *Tavani et al.* [2011], we assumed that extremely high electric fields could be produced during the leader stepping process. Whether such a field magnitude is required in the mechanism we suggest, or can exist in the lightning leader tip region, is an open question that requires further investigation. Additionally, a significant deviation from the typical RREA spectrum can be obtained only if a high electric potential is present in the lightning leader (we used 350 MV in the present paper). More typical lightning producing TGF should involve electric potentials $U_l \sim 100$ MV [*Xu et al.*, 2012]. Using the formula for the nonequilibrium high-energy cutoff $q_e A \simeq 0.08 \times U_l$ described in section 2.1 leads to $q_e A \simeq 8$ MeV (see equation (14)) that is close to the RREA high-energy cutoff $\mathcal{E}_c \simeq 7$ MeV (see section 4.1.1). This would prevent a strong deviation from the classical RREA spectrum from happening over very short timescales in the case of typical TGFs (see Discussion).

[33] The mechanism presented in this paper introduces new outstanding implications on lightning propagation, production of energetic radiation from lightning [*Moore et al.*, 2001; *Dwyer et al.*, 2003, 2005], production of intense beams of electrons and positrons observed from space [*Dwyer et al.*, 2008; *Briggs et al.*, 2011], neutron production from lightning [*Shah et al.*, 1985; *Tavani et al.*, 2011], and on radiation dose received by passengers and crew members on airplanes [*Dwyer et al.*, 2010], as the source of energetic electrons, X-rays and gamma-rays is much more compact and energetic than that deduced from previous studies.

[34] **Acknowledgments.** This research was supported by the NSF grants AGS-1106779 and AGS-0741589 to Penn State University. The authors acknowledge the Research Computing and Cyberinfrastructure unit of Information Technology Services at the Pennsylvania State University for providing HPC resources and services that have contributed to the research results reported in this paper (http://rcc.its.psu.edu).

[35] Robert Lysak thanks the reviewers for their assistance in evaluating this paper.

References

Babich, L. P., E. N. Donskoy, R. I. Il'Kaev, I. M. Kutsyk, and R. A. Roussel-Dupre (2004), Fundamental parameters of a relativistic runaway electron avalanche in air, *Plasma Phys. Rep.*, *30*, 616–624, doi:10.1134/1.1778437.

Balanis, C. A. (1989), *Advanced Engineering Electromagnetics*, John Wiley, New York.

Bazelyan, E. M., and Y. P. Raizer (2000), *Lightning Physics and Lightning Protection*, Instit. of Phys., Bristol, Pa.

Berger, M. J., J. S. Coursey, M. A. Zucker, and J. Chang (2005), Stopping-Power and Range Tables for Electrons, Protons, and Helium Ions, http://www.nist.gov/pml/data/star/index.cfm, Natl. Instit. of Stand. and Technol., Gaithersburg, Md.

Briggs, M. S., et al. (2010), First results on terrestrial gamma ray flashes from the Fermi Gamma-ray Burst Monitor, *J. Geophys. Res.*, *115*, A07323, doi:10.1029/2009JA015242.

Briggs, M. S., et al. (2011), Electron-positron beams from terrestrial lightning observed with Fermi GBM, *Geophys. Res. Lett.*, *38*, L02808, doi:10.1029/2010GL046259.

Carlson, B. E., N. G. Lehtinen, and U. S. Inan (2007), Constraints on terrestrial gamma ray flash production from satellite observation, *Geophys. Res. Lett.*, *34*, L08809, doi:10.1029/2006GL029229.

Carlson, B. E., N. G. Lehtinen, and U. S. Inan (2009), Terrestrial gamma ray flash production by lightning current pulses, *J. Geophys. Res.*, *114*, A00E08, doi:10.1029/2009JA014531.

Carlson, B. E., N. G. Lehtinen, and U. S. Inan (2010), Terrestrial gamma ray flash production by active lightning leader channels, *J. Geophys. Res.*, *115*, A10324, doi:10.1029/2010JA015647.

Celestin, S., and V. P. Pasko (2010), Soft collisions in relativistic runaway electron avalanches, *J. Phys. D Appl. Phys.*, *43*, 315206, doi:10.1088/00223727/43/31/315206.

Celestin, S., and V. P. Pasko (2011), Energy and fluxes of thermal runaway electrons produced by exponential growth of streamers during the stepping of lightning leaders and in transient luminous events, *J. Geophys. Res.*, *116*, A03315, doi:10.1029/2010JA016260.

Celestin, S., and V. P. Pasko (2012), Compton scattering effects on the duration of terrestrial gamma-ray flashes, *Geophys. Res. Lett.*, *39*, L02802, doi:10.1029/2011GL050342.

Coleman, L. M., and J. R. Dwyer (2006), Propagation speed of runaway electron avalanches, *Geophys. Res. Lett.*, *33*, L11810, doi:10.1029/2006GL025863.

Connaughton, V., et al. (2010), Associations between Fermi Gamma-ray Burst Monitor terrestrial gamma ray flashes and sferics from the World Wide Lightning Location Network, *J. Geophys. Res.*, *115*, A12307, doi:10.1029/2010JA015681.

Cummer, S. A., G. Lu, M. S. Briggs, V. Connaughton, S. Xiong, G. J. Fishman, and J. R. Dwyer (2011), The lightning-TGF relationship on microsecond timescales, *Geophys. Res. Lett.*, *38*, L14810, doi:10.1029/2011GL048099.

Dwyer, J. R. (2004), Implications of X-ray emission from lightning, *Geophys. Res. Lett.*, *31*, L12102, doi:10.1029/2004GL019795.

Dwyer, J. R. (2008), Source mechanisms of terrestrial gamma-ray flashes, *J. Geophys. Res.*, *113*, D10103, doi:10.1029/2007JD009248.

Dwyer, J. R., and L. P. Babich (2011), Low-energy electron production by relativistic runaway electron avalanches in air, *J. Geophys. Res.*, *116*, A09301, doi:10.1029/2011JA016494.

Dwyer, J. R., and D. M. Smith (2005), A comparison between Monte Carlo simulations of runaway breakdown and terrestrial gamma-ray flash observations, *Geophys. Res. Lett.*, *32*, L22804, doi:10.1029/2005GL023848.

Dwyer, J. R., et al. (2003), Energetic radiation produced during rocket-triggered lightning, *Science*, *299*(5607), 694–697, doi:10.1126/science.1078940.

Dwyer, J. R., et al. (2004), A ground level gamma-ray burst observed in association with rocket-triggered lightning, *Geophys. Res. Lett.*, *31*, L05119, doi:10.1029/2003GL018771.

Dwyer, J. R., et al. (2005), X-ray bursts associated with leader steps in cloud-to-ground lightning, *Geophys. Res. Lett.*, *32*, L01803, doi:10.1029/2004GL021782.

Dwyer, J. R., B. W. Grefenstette, and D. M. Smith (2008), High-energy electron beams launched into space by thunderstorms, *Geophys. Res. Lett.*, *35*, L02815, doi:10.1029/2007GL032430.

Dwyer, J. R., D. M. Smith, M. A. Uman, Z. Saleh, B. Grefenstette, B. Hazelton, and H. K. Rassoul (2010), Estimation of the fluence of high-energy electron bursts produced by thunderclouds and the resulting radiation doses received in aircraft, *J. Geophys. Res.*, *115*, D09206, doi:10.1029/2009JD012039.

Fishman, G. J., et al. (1994), Discovery of intense gamma-ray flashes of atmospheric origin, *Science*, *264*(5163), 1313–1316.

Fishman, G. J., et al. (2011), Temporal properties of the terrestrial gamma-ray flashes from the Gamma-Ray Burst Monitor on the Fermi Observatory, *J. Geophys. Res.*, *116*, A07304, doi:10.1029/2010JA016084.

Gjesteland, T., N. Østgaard, A. B. Collier, B. E. Carlson, M. B. Cohen, and N. G. Lehtinen (2011), Confining the angular distribution of terrestrial gamma ray flash emission, *J. Geophys. Res.*, *116*, A11313, doi:10.1029/2011JA016716.

Grefenstette, B. W., D. M. Smith, J. R. Dwyer, and G. J. Fishman (2008), Time evolution of terrestrial gamma ray flashes, *Geophys. Res. Lett.*, *35*, L06802, doi:10.1029/2007GL032922.

Gurevich, A. V., G. M. Milikh, and R. A. Roussel-Dupré (1992), Runaway electron mechanism of air breakdown and preconditioning during a thunderstorm, *Phys. Lett. A.*, *165*(5–6), 463–468, doi:10.1016/03759601(92)90348–P.

Howard, J., M. A. Uman, C. Biagi, D. Hill, V. A. Rakov, and D. M. Jordan (2011), Measured close lightning leader-step electric field–derivative waveforms, *J. Geophys. Res.*, *116*, D08201, doi:10.1029/2010JD015249.

Kim, Y.-K., J. P. Santos, and F. Parente (2000), Extension of the binary-encounter-dipole model to relativistic incident electrons, *Phys. Rev. A*, *62*, 052710, doi:10.1103/PhysRevA.62.052710.

Lehtinen, N. G. (2000), Relativistic runaway electrons above thunderstorms, PhD thesis, Stanford Univ., Standford, Calif.

Lu, G., R. J. Blakeslee, J. Li, D. M. Smith, X.-M. Shao, E. W. McCaul, D. E. Buechler, H. J. Christian, J. M. Hall, and S. A. Cummer (2010), Lightning mapping observation of a terrestrial gamma-ray flash, *Geophys. Res. Lett.*, *37*, L11806, doi:10.1029/2010GL043494.

Lu, G., S. A. Cummer, J. Li, F. Han, D. M. Smith, and B. W. Grefenstette (2011), Characteristics of broadband lightning emissions associated with terrestrial gamma ray flashes, *J. Geophys. Res.*, *116*, A03316, doi:10.1029/2010JA016141.

Marisaldi, M., et al. (2010), Detection of terrestrial gamma ray flashes up to 40 MeV by the AGILE satellite, *J. Geophys. Res.*, *115*, A00E13, doi:10.1029/2009JA014502.

Marshall, T. C., M. P. McCarthy, and W. D. Rust (1995), Electric field magnitudes and lightning initiation in thunderstorms, *J. Geophys. Res.*, *100*, 7097–7103, doi:10.1029/95JD00020.

Moore, C. B., K. B. Eack, G. D. Aulich, and W. Rison (2001), Energetic radiation associated with lightning stepped-leaders, *Geophys. Res. Lett.*, *28*(11), 2141–2144, doi:10.1029/2001GL013140.

Moss, G. D., V. P. Pasko, N. Liu, and G. Veronis (2006), Monte Carlo model for analysis of thermal runaway electrons in streamer tips in transient luminous events and streamer zones of lightning leaders, *J. Geophys. Res.*, *111*, A02307, doi:10.1029/2005JA011350.

Østgaard, N., T. Gjesteland, J. Stadsnes, P. H. Connell, and B. Carlson (2008), Production altitude and time delays of the terrestrial gamma flashes: Revisiting the Burst and Transient Source Experiment spectra, *J. Geophys. Res.*, *113*, A02307, doi:10.1029/2007JA012618.

Rakov, V. A., and M. A. Uman (2003), *Lightning: Physics and Effects*, Cambridge Univ. Press, Cambridge, U. K.

Shah, G. N., H. Razdan, Q. M. Ali, and C. L. Bhat (1985), Neutron generation in lightning bolts, *Nature*, *313*, 773–775, doi:10.1038/313773a0.

Shao, X.-M., T. Hamlin, and D. M. Smith (2010), A closer examination of terrestrial gamma-ray flash-related lightning processes, *J. Geophys. Res.*, *115*, A00E30, doi:10.1029/2009JA014835.

Smith, D. M., L. I. Lopez, R. P. Lin, and C. P. Barrington-Leigh (2005), Terrestrial gamma-ray flashes observed up to 20 MeV, *Science*, *307*(5712), 1085–1088.

Smith, D. M., et al. (2011), The rarity of terrestrial gamma-ray flashes, *Geophys. Res. Lett.*, *38*, L08807, doi:10.1029/2011GL046875.

Stanley, M. A., X.-M. Shao, D. M. Smith, L. I. Lopez, M. B. Pongratz, J. D. Harlin, M. Stock, and A. Regan (2006), A link between terrestrial gamma-ray flashes and intracloud lightning discharges, *Geophys. Res. Lett.*, *33*, L06803, doi:10.1029/2005GL025537.

Tavani, M., et al. (2011), Terrestrial gamma-ray flashes as powerful particle accelerators, *Phys. Rev. Lett.*, *106*(1), 018501, doi:10.1103/PhysRevLett.106.018501.

Xu, W., S. Celestin, and V. P. Pasko (2012), Source altitudes of terrestrial gamma-ray flashes produced by lightning leaders, *Geophys. Res. Lett.*, *39*, L08801, doi:10.1029/2012GL051351.